MNRAS **000**, 1–15 (2016) Preprint 18 May 2016 Compiled using MNRAS LATEX style file v3.0

Optimising commensality of radio continuum and spectral line observations in the era of the SKA

Natasha Maddox[1⋆], M. J. Jarvis[2,3], T. A. Oosterloo[1,4]
[1]*ASTRON, the Netherlands Institute for Radio Astronomy, Postbus 2, 7990 AA, Dwingeloo, The Netherlands*
[2]*Oxford Astrophysics, Denys Wilkinson Building, University of Oxford, Keble Rd, Oxford, OX1 3RH, UK*
[3]*Physics Department, University of the Western Cape, Cape Town, 7535, Republic of South Africa*
[4]*Kapteyn Astronomical Institute, University of Groningen, PO Box 800, 9700 AV Groningen, The Netherlands*

arXiv:1605.04962v1 [astro-ph.GA] 16 May 2016

Accepted XXX. Received YYY; in original form ZZZ

ABSTRACT

The substantial decrease in star formation density from $z = 1$ to the present day is curious given the relatively constant neutral gas density over the same epoch. Future radio astronomy facilities, including the SKA and pathfinder telescopes, will provide pioneering measures of both the gas content of galaxies and star formation activity over cosmological timescales. Here we investigate the commensalities between neutral atomic gas (H I) and radio continuum observations, as well as the complementarity of the data products. We start with the proposed H I and continuum surveys to be undertaken with the SKA precursor telescope MeerKAT, and building on this, explore optimal combinations of survey area coverage and depth of proposed H I and continuum surveys to be undertaken with the SKA1-MID instrument. Intelligent adjustment of these observational parameters results in a tiered strategy that minimises observation time while maximising the value of the dataset, both for H I and continuum science goals. We also find great complementarity between the H I and continuum datasets, with the spectral line H I data providing redshift measurements for gas-rich, star-forming galaxies with stellar masses $M_* \sim 10^9\ M_\odot$ to $z \sim 0.3$, a factor of three lower in stellar mass than would be feasible to reach with large optical spectroscopic campaigns.

Key words: surveys–galaxies:general–galaxies:evolution–radio continuum: galaxies–radio lines:galaxies

1 INTRODUCTION

The dramatic decrease in the cosmic star formation density from $z = 1$ to the present day has been well documented (see Hopkins & Beacom 2006, for example). Conversely, the neutral gas content (H I) of galaxies spanning the same redshift range is much less well known. At $z \sim 0$, large area surveys such as the Arecibo Legacy Fast ALFA survey (ALFALFA, Giovanelli et al. 2005) and the H I Parkes All-Sky Survey (HIPASS, Barnes et al. 2001, Meyer et al. 2004) provide direct detections of the cold neutral gas in galaxies, from which the H I density of the local Universe can be derived. Targeted studies, such as the Blind Ultra-Deep H I Environmental Survey (BUDHIES, Jaffé et al. 2013), or the HIGHz survey (Catinella & Cortese 2015), have used many hundreds of hours of observing time to detect several galaxies in H I at $z \sim 0.2$, but the detected objects are not representative of the general galaxy population, being either located in high density environments, or lying at the upper end of the galaxy mass distribution. An average measurement of the H I content of galaxies not individually directly detected can be derived from spectral stacking, which has provided estimates of the cosmic H I density to $z \sim 0.2$ (Lah et al. 2007, and Rhee et al. 2013, for example), and can be extended to even higher redshifts.

At high ($z > 1$) redshifts, the neutral gas content of galaxies and their environments is detected in absorption along the line-of-sight toward background quasars, resulting in damped Lyα systems (DLAs), lower column density Lyman limit systems and the Lyα forest. The large numbers of these systems currently known (several thousands, see Noterdaeme et al. 2012) gives an indirect measurement of the gas content of galaxies at redshifts beyond the reach of current radio telescopes. The lower redshift limit of $z \sim 1$ is set by the Lyα absorption appearing in the ultra-violet, necessitating expensive space-based spectroscopy.

⋆ E-mail: maddox@astron.nl

© 2016 The Authors

As H I provides the fuel for star formation, a connection between star formation activity and the neutral gas reservoirs available to feed the activity is expected. An intriguing detail is that while the level of star formation has dropped by more than an order of magnitude from $z = 1$ to the local Universe, the difference between the H I density at $z = 0$ measured from H I in emission to $z > 1$ measured from H I in absorption has only changed by a factor of a few (see Rhee et al. 2013, for example). The nearly constant H I density since $z = 1$ indicates replenishment of the gas reservoir, as the gas consumption timescales are relatively short in comparison. This discrepancy also points to at least one additional ingredient required to connect the reservoir of fuel to stellar buildup. Molecular gas, as the intermediary between neutral gas and star formation, is an obvious line of investigation. ALMA, with its exceptional sensitivity, is revolutionizing the study of molecular gas, both at low and high redshift.

Observing H I in emission spanning the redshift range $0 < z < 1$ is within the capabilities of the next generation of radio telescopes, and is one of the key science cases for the Square Kilometre Array (SKA, Braun et al. 2015). In the meantime, existing facilities, including the recently upgraded Karl G. Jansky Very Large Array (VLA), and the APERture Tile in Focus (APERTIF) focal-plane array system planned for deployment on the Westerbork Synthesis Radio Telescope in 2016 (Oosterloo et al. 2009), will allow measurement of the H I content of galaxies to $z = 0.45$ and $z = 0.25$, respectively. A deep H I survey, the COSMOS H I Large Extragalactic Survey (CHILES) is indeed already underway with the VLA (see Section 4.5).

In preparation for the SKA, mid-frequency pathfinder radio telescopes currently under construction including South Africa's MeerKAT (Jonas 2009) and the Australian Square Kilometre Array Pathfinder (ASKAP, Johnston et al. 2008), will improve on the capabilities of existing facilities. Thus, we will be able to begin exploring the gap in redshift, $0 < z < 1$, corresponding to lookback times up to nearly 8 Gyr, which has thus far remained almost entirely inaccessible with respect to the neutral gas content of galaxies.

1.1 Commensality and complementarity

In practice, the amount of time available on a given facility is finite. Performing observations *commensally*, i.e. multiple independent projects with distinct science goals all using the data from a single observation, greatly improves the efficiency of a telescope. Clever adjustment of the observational parameters, including integration time, survey area, and frequency resolution, enables maximum scientific return for a given dataset. We focus here on the commensality between H I and continuum observations, with the aim of optimising the scientific return for the H I surveys, by adjusting only the depths and areas of the observations. The ability to combine surveys with historically different observation modes, namely spectral line and radio continuum, has only recently become feasible due to expanded bandwidth of receivers and sufficient computing to handle the increased data rates. Previously, observing in spectral line mode was necessarily restricted to a limited frequency range, corresponding to a very narrow volume slice, appropriate for targeted observations. Performing purely commensal continuum observations in spectral line mode was not worth the increased computing overhead, because the probability of the small volume probed containing an H I-rich galaxy was low. With the increased bandwidth available for spectral line observations, spanning many hundreds of MHz, the volume probed for H I detections is vastly increased.

We note that the different computing requirements of spectral line and continuum science, with respect to imaging, spatial and spectral resolution, among other things, will need to be considered. Spatial and spectral resolution can be customized for each science case by implementing this flexibility within the data processing pipeline. Fortunately, the H I and continuum observations have similar initial calibration requirements, so the computing overhead for processing a set of observations to be suitable for both H I and continuum science is minimal.

Satisfying the observational requirements of multiple science cases while staying within the boundary conditions of available observing time requires careful planning and preparation. We should also be mindful of existing and planned ancillary data efforts. Survey area, depth, and particularly relevant for radio observations, spatial resolution, need to be considered. At the depths probed by next generation radio facilities, the continuum source density is high (Jarvis et al. 2015), requiring adequate spatial resolution, of the order of an arcsecond or less, to avoid source confusion. The H I source density is much lower, and thus confusion is not as problematic.

We also investigate the *complementarity* of the resulting data products. Ultra-deep neutral hydrogen surveys are planned with both MeerKAT (LADUMA, Holwerda et al. 2012) and ASKAP (DINGO[1]), spending several thousands of hours of observations of single fields to detect H I in galaxies to higher redshifts and lower H I masses than possible with existing telescopes. These same observations will be used by the radio continuum teams, who intend to create ultra-deep continuum maps using multi-frequency synthesis imaging. The converse is also true, with H I spectral line data to be extracted from large area continuum observing programmes. Thus, from the same observations, simultaneous H I spectral line and broad-band continuum data can be obtained, probing both the neutral gas reservoirs and star formation activity for a large sample of galaxies spanning a cosmologically significant range in redshift. This dual-usage of a single dataset to explore two related, yet distinct, physical processes is unique to upcoming radio surveys.

We focus only on surveys using the MeerKAT pathfinder and the SKA Phase 1 mid-frequency (SKA1-MID) instrument. We have not included proposed APERTIF or ASKAP surveys, as the final performance of the phased array feeds emerging technology has yet to be conclusively measured. Also, while the single pointing field of view is $\sim$30 deg^2, the frequency range, and thus redshift range accessible for H I, will not be as extensive as that of MeerKAT or SKA1-MID.

The current work has two goals. The first is to investigate commensal observations, focusing on a combination of surveys soon to begin, in Section 2. We then use what

[1] http://www.physics.uwa.edu.au/~mmeyer/dingo

we learned from that example to suggest optimal commensality for upcoming SKA surveys in Section 3, and focus on parametrization of the H I mass function as a general science goal. The investigation here serves as input for the ongoing discussion regarding the definition of the surveys to be undertaken with next generation facilities. In the second half of the work, starting in Section 4, we focus on how H I spectral line and radio continuum observations are complementary, and what information each provides with respect to the other. A case study for a pair of surveys currently underway is in Section 4.5. A summary is in Section 5. Concordance cosmology with $H_0 = 70$ km s^{-1} Mpc^{-1} (thus $h \equiv H_0/[100$ km s^{-1} Mpc$^{-1}] = 0.7$), $\Omega_m = 0.3$, $\Omega_\Lambda = 0.7$ is assumed when computing masses and luminosities, unless noted otherwise.

2 COMMENSAL H I AND CONTINUUM SURVEYS

Advances in computing power and engineering technology provide flexibility in observing techniques. In the past, observations were performed either in spectral line mode, with fine spectral resolution over a limited frequency range, or continuum mode, with coarser spectral resolution over a wider frequency range. Upcoming facilities will have no such restriction, enabling simultaneous spectral line and continuum observations. While this is clearly efficient with respect to observing time, the science return of the observations can also be increased.

2.1 LADUMA and MIGHTEE with MeerKAT

The South African SKA precursor facility, MeerKAT, is a 64-element array of 13.5 m dishes located in the Karoo region of South Africa. The smaller dish diameter of MeerKAT, with respect to the VLA, results in a larger field of view (FoV), with the primary beam full width half maximum (FWHM) of nearly 1 degree at 1420MHz for the former compared to 0.5 degree for the latter. The majority of operational time has been allocated to several large programmes, with the remaining time available for smaller individual projects.

Looking At the Distant Universe with the MeerKAT Array (LADUMA), is the deep H I survey to be undertaken with MeerKAT. LADUMA has been allocated 5000 hours of observing time for a single pointing, to be split between two frequency bands, covering $0 < z < 0.58$ for H I (1670–900 MHz) in Phase 1 operations, and $0.40 < z < 1.4$ (1015–580 MHz) in Phase 2.

The MeerKAT International Giga-Hertz Tiered Extragalactic Exploration (MIGHTEE; Jarvis 2012) survey is the MeerKAT continuum key science survey, and follows a wedding-cake design. The exact parameters are yet to be finalised, but for our purposes here, we assume a medium-deep layer covering 35 deg^2, and a deep $\sim$1 deg^2 component coincident with the LADUMA pointing. The final area coverage will not change significantly from these values. The observations allocated to LADUMA will be made available to the MIGHTEE team for continuum science, while the data collected for MIGHTEE can be used for H I science, as it will be collected in spectral line mode, with velocity resolution of 26kHz, corresponding to 5.5 km s^{-1} at $z = 0$ for H I, increasing to 7.8 km s^{-1} at $z = 0.4$. Thus, LADUMA and MIGHTEE are to be observed entirely commensally.

2.1.1 *LADUMA as MIGHTEE Deep*

The 5000 hours of integration for LADUMA is sufficient to directly detect the most H I-massive systems at $z = 0.6$ and beyond. This does not, however, directly imply that the continuum data will reach depths corresponding to such long integration times. The longest planned baseline of the MeerKAT array is 8 km, resulting in spatial resolution ranging from $\sim 6''$ at 1420MHz to $>15''$ at 600MHz. Using the approximation listed in equation 27 in Condon et al. (2012) to compute the noiseless confusion distribution width $\sigma_c^\star$, the continuum confusion noise is $\sim 1 \mu$Jy beam^{-1} for these resolutions, which is reached in approximately 50 hours with MeerKAT, and cannot be overcome without introducing longer baselines.

A more significant contribution that LADUMA data can make to the MIGHTEE project is by providing redshifts for the H I-rich, but relatively low stellar mass galaxies at $z < 0.4$, which will have significant levels of star formation, but are optically faint, and therefore difficult spectroscopic targets at visible wavelengths.

2.1.2 *MIGHTEE as LADUMA Wide*

While LADUMA provides a deep continuum pointing for MIGHTEE, MIGHTEE provides complementary wide-area H I data with observations covering 35 deg^2, with tens of hours of integration per pointing. This is clearly not comparable to the thousands of hours devoted to LADUMA, but it is sufficient to detect the most massive H I systems, which will be under-represented in the relatively small volume contained within a single pointing. These same gas-rich galaxies will also have significant star formation, and thus will be a prominent population within the MIGHTEE continuum dataset. We will then have simultaneous measures of the neutral gas content and star formation rates of galaxies extending beyond $z \sim 0$, including a wide range of environments, as the volume probed is large enough to include a number of massive clusters. The benefits of using the medium-deep continuum survey data to supplement H I surveys is expanded and investigated in the following section.

2.2 Galaxy counts and redshift distribution

Here we make qualitative predictions of what we can expect from planned surveys and how we can best combine the available information. In the absence of direct observations of the H I content of galaxies at $z > 0.2$, we rely on information gathered from the low redshift Universe, combined with simulations, to estimate the number of galaxies, and their distribution in mass and redshift, upcoming surveys will detect.

We start by investigating the LADUMA–MIGHTEE survey combination, focusing on the H I aspect, as this is where the greatest complementarity is seen. The confusion issues for the continuum observations make a similar analysis

much more complex. For the following, we use the information provided to the public for MeerKAT[2]. The listed System Equivalent Flux Density (SEFD) values indicate MeerKAT's performance is expected to be better than that of the VLA, possibly by as much as a factor of two in sensitivity.

As listed in Table 1, for the low redshift (Phase 1) component of LADUMA, the integration time will be 1000 hours, which corresponds to a 5-σ H I flux limit of 0.015 Jy km s^{-1} for MeerKAT over 250 km s^{-1}. We choose this profile width as we expect the majority of detected objects to be massive systems, with profiles that can easily span several hundreds of km s^{-1}. Equivalently, for 24 hours per MIGHTEE pointing, the 5-σ H I flux limit is 0.07 Jy km s^{-1}. We assume that the full 35 deg^2 area will be composed of 35 individual pointings, instead of a single mosaic, which removes the complication of an increasing effective exposure time for a given patch of sky within a mosaic, as the primary beam increases in size going to lower frequency, and hence to higher redshift, and the individual pointings increasingly overlap. We note, however, that in practice there will be overlap between some of the pointings, thus the calculations here are conservative with respect to the mass detection limit.

We use the parameters from the analytic fits to the dN/dz relations derived from the simulations of Obreschkow et al. (2009) to convert flux limits in H I to numbers of galaxies detected as a function of redshift. The simulations are consistent with the observed $z = 0$ H I mass function and CO(1–0) luminosity function, and allow for evolution of the H I content of galaxies with redshift. The dN/dz relations enable us to determine, for a given redshift shell and sky area, the total number of galaxies expected to be detected above a specified flux limit. Appropriate relations for arbitrary integrated flux limits can be obtained by interpolating the function coefficients for the given set of flux limits. We note that the dN/dz relations are based on the cosmological parameters of $H_0 = 100h$ km s^{-1} Mpc^{-1} with $h = 0.73$, $\Omega_m = 0.25$ and $\Omega_\Lambda = 0.75$ (Spergel et al. 2003), which have been superceded by, for example, Komatsu et al. (2011), but the effect on the results is negligible.

We also make use of the H I mass function (HIMF) derived at $z \sim 0$ from ALFALFA (Martin et al. 2010), which spans $6 < \mathrm{Log}(M_{HI}) < 11$. Galaxies with $M_{HI} > 10^{11}$ M$_\odot$ are exceedingly rare, so we do not include them in our calculations. From the H I mass function, we can estimate how the galaxies in each redshift shell are distributed in mass. For the single MeerKAT pointing of LADUMA and 35 deg^2 of MIGHTEE, we can compute how many galaxies of each mass we expect to observe over the full survey redshift range. Fig. 1 shows the result of this exercise, limited to $z < 0.4$. As seen, the continuum survey, MIGHTEE, detects nearly three times as many galaxies in H I as the deep H I survey, LADUMA, due to the larger area, and thus larger volume, surveyed. The difference is particularly notable at the high H I-mass end, where very few massive H I systems are detected by LADUMA.

Fig. 2 shows how the detected galaxies counted in Fig. 1 are distributed in the redshift–M_{HI} plane. The plane is divided into cells of width Δz=0.01 and $\Delta\mathrm{Log}(M_{HI})$=0.1. The contours for both LADUMA and MIGHTEE are set at 1, 10 and 25 galaxies per cell. Complications due to spatial resolution determined by the size of the synthesized beam, how this size changes with redshift, and the resulting effect on column density sensitivity have been neglected for this exercise. The sensitivity is maximized when the size of the galaxy matches the size of the beam, and decreases for larger and smaller sources. Therefore, the lower boundaries of detected galaxies are specifically for galaxies the same size as the beam, and extends to higher masses for galaxies of smaller or larger physical sizes.

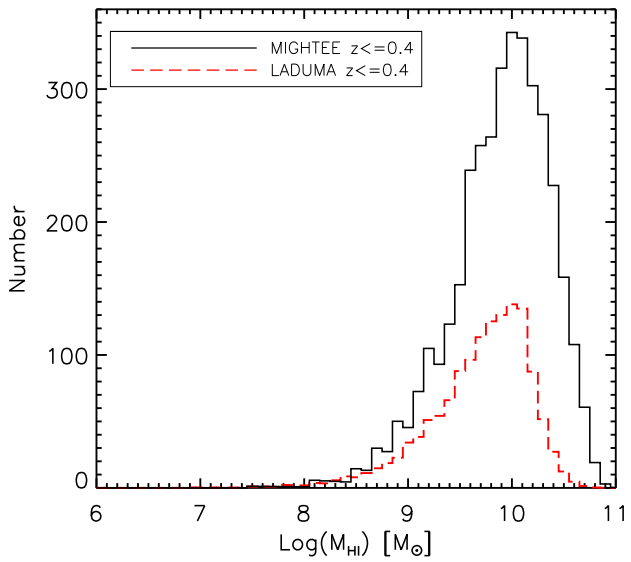

Figure 1. Number of galaxies as a function of H I mass observed in the single pointing of LADUMA, (red dashed line), and in the 35 deg^2 of MIGHTEE (black solid line), both for $0 < z < 0.4$.

The two MeerKAT surveys are highly complementary, with MIGHTEE primarily detecting high H I mass galaxies at low redshift, while LADUMA reaches further down the H I mass function. This access to wide area will constrain the high mass end of the H I mass function, which is populated by galaxies with low space density. The wide area is also essential for studies of galaxy environment and large scale structure, which are inaccessible to the narrow, deep observations. Thus, including H I data from the continuum survey greatly enhances the potential scientific output of the H I studies.

3 SKA PHASE I COMMENSAL SURVEY DESIGN

A tiered, or "wedding-cake", survey design, is often employed by large projects, as it provides dynamic range in depth, while also probing a large volume. The relative depths of the tiers must be set to provide optimal coverage of some parameter of interest. Here we investigate surveys suggested to be undertaken with SKA1-MID. The facility will be a combination of 133 15 m new SKA dishes, in addition to the 64 13.5 m MeerKAT dishes, as outlined in the Baseline

[2] http://public.ska.ac.za/meerkat/meerkat-schedule, Released 08 Dec 2015

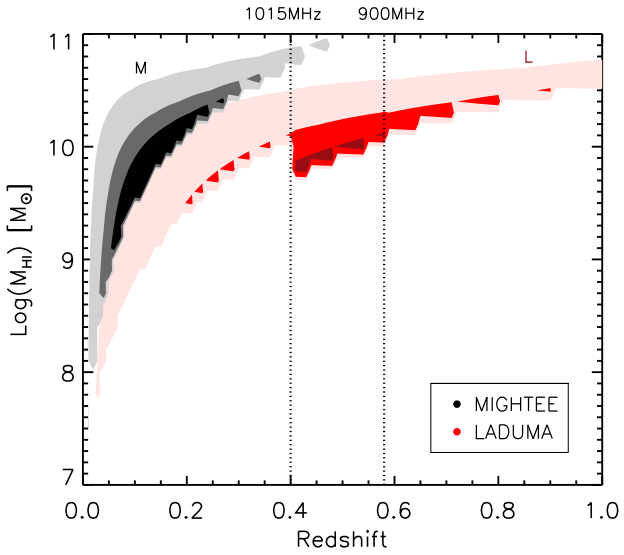

Figure 2. The coverage in the redshift–M_{HI} plane for LADUMA (red contours, with 'L' label) and MIGHTEE (greyscale contours, with 'M' label). The parameter space is divided into cells of width 0.01 in redshift and 0.1 in Log(M_{HI}). The contour levels for both surveys are the same, surrounding regions of parameter space containing at least one (faint shading), 10 (medium shading), and 25 (dark shading) galaxies per cell. Due to the overlapping frequency coverage of the two MeerKAT receivers, the redshift range $0.40 < z < 0.58$ is observed for the full 5000 hours for LADUMA, and is correspondingly deeper.

Design Document Version 2[3]. As the final telescope will be composed of two types of dishes, each with their own performance characteristics, accurately anticipating the sensitivity of SKA1-MID is difficult. However, given the SEFD values provided in the Baseline Design Document for the SKA dishes, and those provided in the public MeerKAT documentation, we conservatively estimate a factor of 5 increase in sensitivity of SKA1-MID Bands 1 and 2, with respect to the VLA, consistent with simulations by Popping et al. (2015).

We construct the survey tiers keeping in mind that the resulting data will be used commensally by both the H I and continuum teams, and thus restrict ourselves to the range of parameters that are useful to both. We use the sensitivity to H I mass as a function of redshift as a measure of the value of the survey tier combination, and optimise the tiers by rearranging their depth and area to maximise coverage of the redshift–M_{HI} plane.

3.1 Optimal SKA Survey Tiers

The redshift and H I mass distribution of galaxies expected from surveys displayed as in Fig. 2 can be used as a powerful diagnostic tool to explore combinations of depth and area which result in the most scientifically useful dataset. LADUMA and MIGHTEE are clearly well paired at $z < 0.4$, enhancing the usefulness of the data.

The SKA H I science working group (SWG) proposed a tiered observing strategy to be undertaken with SKA1-MID to address many extragalactic H I science cases, consisting of an ultra-deep, small area survey, a medium-wide, medium-deep survey, and a wide-area, relatively shallow survey. We refer to these three tiers as Ultra-Deep (UD), Medium-Wide (MW) and Wide (W). Their areas, integration times and approximate 5-σ sensitivities that can be expected are listed in Table 1 as the "Fiducial" case, as set by (Staveley-Smith & Oosterloo 2015). A more detailed discussion within the H I SWG of the three tiers will come at a later date, when the technical specifications of the SKA1-MID are better known, but the suggested Fiducial case serves as a useful starting point. We have not included the "strawman" surveys outlined in the SKA H I galaxy evolution chapter (Blyth et al. 2015), as they rely heavily on the SKA-SURVEY instrument, construction of which has been deferred.

We show in Fig. 3 the coverage in the redshift–M_{HI} plane resulting from the three Fiducial H I survey tiers. Increasing the integration time to 4000 hours per tier, to be consistent with the proposed surveys discussed below, improves the sensitivity by a factor of two, but the general features remain unchanged.

A critical aspect missing from the H I SWG observing strategy is the possibility of observing commensally, in particular sharing observations with the SKA continuum SWG (Prandoni & Seymour 2015). While commensal observing necessarily involves some compromises to be made on some aspects, including field selection, the benefits are significant, including the increased available observing time.

The continuum SWG also proposed a three-tiered observing strategy, with areas comparable to those explored here, with a single pointing UD tier, a MW tier spanning 10–30 deg^2, and a W tier of $\sim$1000 deg^2. The suggested continuum RMS values for the three tiers of 0.05, 0.2 and 1μJy, respectively, can be compared with the estimated RMS values computed for the Fiducial and Optimised surveys as listed in Table 1. We do not list continuum RMS values for the Requested or Ideal cases, because the relevant receivers do not currently exist.

We suggest a number of tiered survey strategies working within the framework of commensal extragalactic H I and continuum observations. The three tiers under consideration are driven by different science cases. The UD tier is driven primarily by the redshift evolution of H I science case, and has very little flexibility. In order to detect the faintest objects at the greatest distances, long integration times are required. The deepest integration is achieved by observing only a single pointing, the area of which is set by the FoV of the telescope. At the other extreme, the W tier is of general use for many science cases. The size is restricted by the amount of area that can be covered with individual pointings long enough such that they are not dominated by calibration overheads. The MW tier is intermediate between the two, and requires advance planning to maximise the scientific return. The area and depth must be simultaneously adjusted such that a representative volume containing detectable galaxies is observed.

For our purposes, we assume in the following that the continuum science will be the primary driver behind the MW tier, as it will provide the bulk of the continuum science return. The W tier is too shallow to explore

[3] https://www.skatelescope.org/key-documents/, Released October 2015

Table 1. Parameters for the two MeerKAT surveys, LADUMA (Phase 1) and MIGHTEE, and the four different combinations of survey tiers suggested for the SKA Phase 1 MID instrument. The confusion noise floor of $\sim 1\mu$Jy for MeerKAT limits the continuum depth of LADUMA and MIGHTEE. The Fiducial case is from the SKA H I Science Working Group, whereas the Optimised case alters the depth and areas of these three tiers. The Requested case reflects the frequency coverage of the suggested revised Band 1 and Band 2, while the Ideal case is for a hypothetical, single-octave receiver system. For the Optimized and Ideal cases, the UD tier is two pointings covering the same redshift range, to alleviate cosmic variance. For the Requested case, the two UD pointings are split between Bands 1 and 2. T_{exp} is the effective integration time per pointing, and the H I flux limits assume SKA1-MID sensitivity 5 times that of the VLA and profile widths of 250 km s^{-1}. Continuum RMS values for the UD tiers assume Band 1, and Band 2 for MW and Wide. The combination of lower SEFD and wider available bandwidth for Band 2 with respect to Band 1 results in similar RMS values for the UD and MW tiers for the Optimised case.

Name	Area deg^2	T_{exp} hours	H I 5-σ Jy km s^{-1}	Continuum RMS μJy
LADUMA	1	1000	0.015	1
MIGHTEE	35	24	0.07	1
Fiducial				
UD	1	1000	0.003	0.07
MW	20	50	0.014	0.14
Wide	400	2.5	0.06	0.64
Optimised				
UD	2	2000	0.002	0.05
MW	10	400	0.0047	0.05
Wide	1000	4	0.05	0.51
Requested				
UD	2	2000	0.002	
MW	30	50	0.014	
Wide	1000	4	0.05	
Ideal				
UD	2	2000	0.002	
MW	30	50	0.014	
Wide	1000	4	0.05	

a signficant redshift range, while the narrow UD tier will suffer from cosmic variance, which becomes a significant source of uncertainty for areas smaller than about 10 deg^2 (Heywood, Jarvis, & Condon 2013). This is consistent with the SKA continuum SWG specification that the MW tier should be 10–30 deg^2, while the required sensitivity should be sufficient to sample the peak of star formation, at $1 < z < 3$.

Continuum confusion is not an issue for SKA1-MID as it is for MeerKAT and ASKAP, as the array layout will enable sub-arcsecond spatial resolution. H I science can employ a range of spatial resolutions, matching the resolution with the angular scale of the targets. We assume that the continuum and H I data processing pipelines will be able to customize the spatial resolution of the respective maps for optimal sensitivity.

A critical aspect of the following investigation is the frequency coverage of the SKA1-MID instrument. The current design for the mid-frequency receivers is for Band 1 to cover

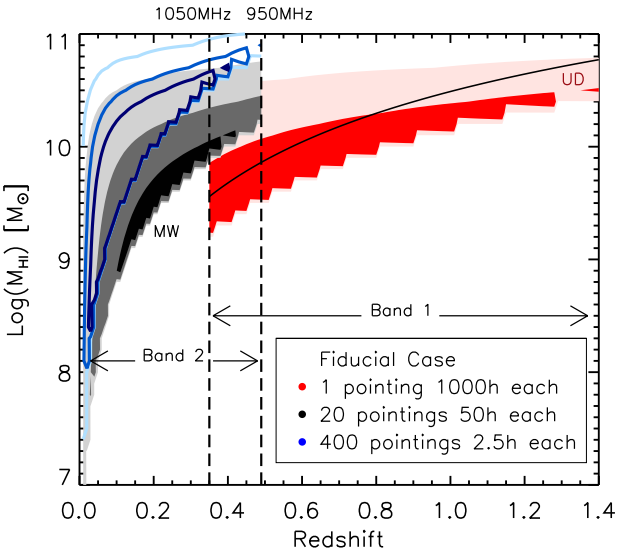

Figure 3. The coverage in the redshift–M_{HI} plane for the Fiducial SKA1 UD (red filled contours, with 'UD' label), MW (greyscale filled contours, with 'MW' label), and W survey (blue open contours). The parameter space is the same as in Fig. 2, but extends to $z = 1.4$. The contour levels for all three surveys are the same, surrounding regions of parameter space containing at least 1 (faint shading), 25 (medium shading), and 100 (dark shading) galaxies per cell. The contours for the wide survey are unfilled to show the overlapping regions between W and MW. The vertical dashed lines indicate the lower edge of Band 1 at 1050MHz, and the upper edge of Band 2 at 950MHz. The black solid curve indicates the H I mass sensitivity if the performance of Band 1 is reduced by a factor of two.

1050–350MHz (corresponding to $0.35 < z < 3$ for H I observations), and Band 2 1700–950MHz ($z < 0.5$), the extent of which are indicated as vertical dashed lines in Fig. 3. H I surveys are particularly affected by the choice of frequency coverage, as it directly dictates the redshift range that can be surveyed in a given observation. This is highlighted by the discontinuity in coverage in Fig. 3 at 1050MHz, or $z < 0.35$, indicating a mismatch in depth between the UD and MW components. Constructing a receiver band such as the current planned Band 1 is a challenging engineering task. We have thus marked on Fig. 3 the equivalent H I mass sensitivity if the Band 1 performance is decreased by a factor of two. Current measurements of the receiver indicate it performs slightly better than this at low redshift (high frequencies), with decreasing sensitivity to high redshift (lower frequencies)[4].

Alternative possibilities for receiver bands are currently under discussion. One option that has been suggested is to replace the current wide Band 1 with a single-octave band covering 875–475MHz ($0.6 < z < 2.0$ for H I), and the low redshift Band 2 with a second band covering 1470–795MHz ($0 < z < 0.8$)[5]. This arrangement shifts the overlapping red-

[4] http://astronomers.skatelescope.org/ska1/
[5] https://skaoffice.atlassian.net/wiki/display/EP/ECP+Register ECP150027

shift range from $0.35 < z < 0.5$ to $0.6 < z < 0.8$. This arrangement is listed as "Requested" in Table 1.

Addtional options involve a single-octave band covering either 1420–710MHz ($0 < z < 1$ for H I), or 1200–600MHz ($0.2 < z < 1.4$). Although the second range excludes observing H I at $z = 0$, it is an attractive option for a number of reasons. First, with respect to survey commensality, detailed H I observations of nearby galaxies have different requirements to the deep H I surveys aiming for higher redshift, so it is sensible to perform the $z = 0$ and $z > 0$ surveys separately. In addition, there is known severe RFI at 1170–1300MHz[6], rendering extracting data from observations within this frequency range very problematic. Continuum studies also stand to benefit, as the lower frequency limit of 600MHz results in a larger FoV and enhances sensitivity due to the spectral shape of radio sources, albeit with poorer spatial resolution. Including coverage at $1.0 < z < 1.4$ at the expense of $z < 0.2$ also offers the opportunity to explore new parameter space, which is only accessible to the SKA. The number of galaxies directly detected at such high redshifts will be modest, but we will gain the most new information with such observations.

In the following, we investigate three cases for frequency coverage. The first assumes the frequency bands as they are currently defined, but optimising survey tier depth and area (Optimised). The second refers to the proposed shifting of the frequency coverage of Bands 1 and 2 (Requested), and the third assumes a single band covering either 1420–710MHz or 1200–600MHz (Ideal). We restrict the total observing time for each survey tier to be nominally one year, which corresponds to approximately 4000 hours of usable integration time.

For the Optimised case, we first fix the UD component, which has very few options for variation. We choose to split the 4000 hours into two pointings instead of one, to alleviate cosmic variance. We are then free to adjust the area and exposure time per pointing of the MW and W components to address the science cases. As a general rule, increasing area improves coverage of the high mass region of redshift–M_{HI} parameter space, whereas increasing integration time improves coverage at lower masses.

Fig. 4 shows how the redshift–M_{HI} plane is populated for the Optimised surveys listed in Table 1, after adjusting the three tiers for optimal coverage in mass and redshift. For this arrangement, in order to maintain high dynamic range in H I mass at low redshifts, the MW tier is necessarily deep, with correspondingly smaller area to keep the total survey time within the 4000 hour budget. 10 deg^2 is at the low end of the range of survey areas deemed to be acceptable for this tier by the SKA continuum SWG (Prandoni & Seymour 2015).

We have increased the area of the wide tier from 400 to 1000 deg^2, which better samples the high-mass end of the H I mass distribution. Increasing the area further would require shorter exposure times per pointing, which we want to avoid. As H I column density sensitivity also scales with exposure time, longer exposures have greater sensitivity to diffuse H I, and therefore can be imaged at higher spatial resolution, than shorter exposures. Short integration times over a larger area, with the accompanying poorer resolution, would not be a significant improvement over currently available technology, and would not efficiently exploit the full capabilities of the SKA.

Fig. 5 shows a combination of survey tiers more appropriate for the Requested frequency coverage. In order to span the full redshift range, the UD tier has been split in two, with one 2000h integration at low redshift (Band 2), and one 2000h integration at high redshift (Band 1). The redshift range $0.6 < z < 0.8$ is covered by both Band 1 and Band 2, and thus receives 4000h of integration, and is subsequently deeper. The primary difference between the Optimised and Requested cases is in the MW tier, which no longer needs to be as deep. In fact, the coverage of the MW tier is achieved by using only 30 pointings of 50 hours each, using only 1500 of the nominally available 4000 hours. 30 deg^2 is also well-matched to the planned survey area of the LSST deep fields, which will cover 36 deg^2 in the first instance. The remaining time beyond 1500 hours could be used to more than double the area covered, if desired.

Fig. 6 shows the alternative arrangement for frequency coverage, listed as Ideal in Table 1, using either the 1420–710MHz or 1200–600MHz single band. Although we display the full redshift range of $0 < z < 1.4$, note that only either the range $0 < z < 1$ or $0.2 < z < 1.4$ can be covered with a single observation. The MW and W tiers are unchanged from the Requested case, but the UD tier is again composed of two, 2000h integrations, which span the full available redshift range.

We emphasize here that, between the Optimised and Requested or Ideal frequency setups, it is the MW tier that is the most effective for optimizing the coverage of the redshift–M_{HI} plane. As the specifications of the MW tier are of critical importance to the continuum SWG, the importance of full investigation of survey commensality becomes apparent.

We have thus far not mentioned the nearby galaxies extragalactic H I science case, which aims to map the neutral gas distribution of a number of local, well-resolved galaxies in much greater detail than will be achieved with either the ultra-deep or wide-area surveys. These targeted observations will observe a small number of fields with long exposure times, similar to the parameters for the MW surveys discussed here. However, these MW observations cannot be easily shared with the local galaxies communities, as the fields would be specifically chosen such that they do *not* have prominent nearby galaxies within them. Although the spectral dimension allows us to see in H I beyond the local galaxies, they are optically opaque, rendering the entire volume beyond the galaxies inaccessible to ancillary data. While there is no clear commensality between the deep extragalactic surveys discussed here and the resolved studies of nearby galaxies, the H I and continuum teams targeting these galaxies will certainly exploit the high degree of commensality between their respective observations.

3.2 Parametrizing the H I Mass Function

With several options for survey design available to us, we need some way of quantifying the quality and usefulness of the resulting dataset. Population studies require dynamic range in mass at a given redshift, whereas evolution studies require dynamic range in redshift at a given mass. H I content as a function of environment requires sufficient sur-

[6] http://public.ska.ac.za/meerkat/meerkat-schedule

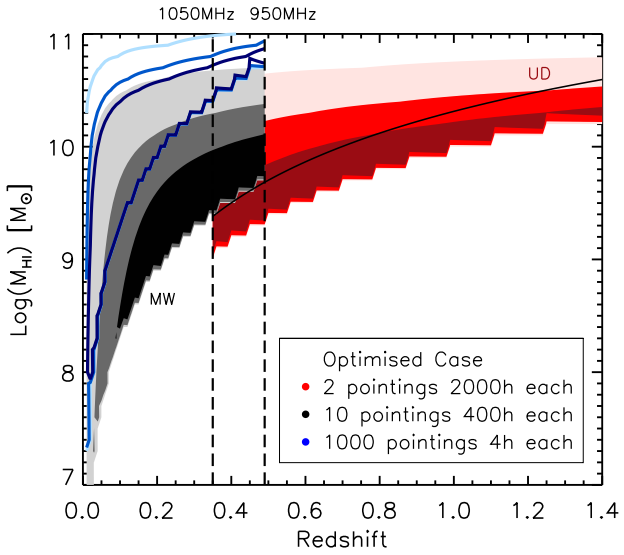

Figure 4. The coverage in the redshift–M_{HI} plane for an SKA1 UD (red filled contours, with 'UD' label), MW (greyscale filled contours, with 'MW' label), and W survey (blue open contours), corresponding to the Optimised case in Table 1. The contour levels for all three surveys are the same, surrounding regions of parameter space containing at least 1 (faint shading), 25 (medium shading), and 100 (dark shading) galaxies per cell. The black solid curve indicates the H I mass sensitivity of Band 1 if it is reduced by a factor of two. The characteristic mass, which is $M_\star = 10^{9.96} M_\odot$ at $z = 0$, is well covered with this set of surveys.

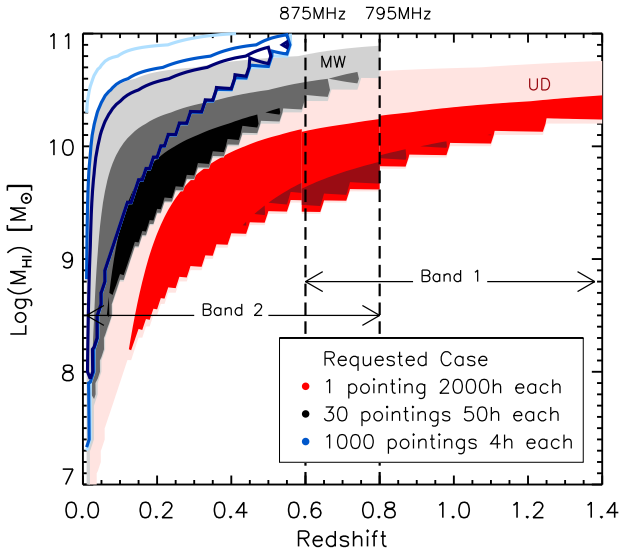

Figure 5. Same as in Fig. 4, but for the frequency band definition corresponding to the Requested case. Note that the UD component now must be built from two separate integrations, one with Band 1 and one with Band 2, while the redshift range $0.6 < z < 0.8$ is observed twice.

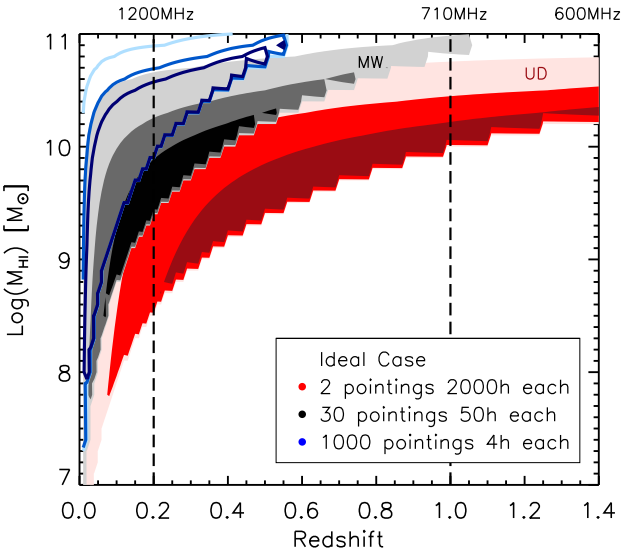

Figure 6. Same as in Fig. 4, but for the frequency band definition corresponding to the Ideal in Table 1. Note that either $0 < z < 1$ or $0.2 < z < 1.4$ can be observed at once, but not the full redshift range $0 < z < 1.4$. The lack of the $z < 0.35$ lower redshift cutoff for the UD component means the MW tier can be shallower and wider, and completed in only 1500 hours. The absence of the $z > 0.5$ upper redshift cutoff enables the MW tier to continue contributing coverage of the high-mass galaxies up to $z = 1$. Either band definition results in a more efficient set of surveys which covers more of the redshift–M_{HI} plane than with the existing Bands 1 and 2.

vey volume to include a range of galaxy group and cluster masses. Applications such as investigating the evolution of the H I mass function with redshift would benefit from coverage of the redshift–M_{HI} plane spanning the break of the relation, which is at $\mathrm{Log}(M_{HI}) = 9.96\ M_\odot$ at $z \sim 0$ (Martin et al. 2010). If continuous coverage of H I mass at a given redshift is a priority, then adjusting exposure times and survey areas can minimize gaps in the redshift–M_{HI} plane.

We have chosen as an illustrative target science goal the characterisation of the H I mass function (HIMF) as a function of redshift. This fundamental relation can be integrated to give the cosmic H I density, Ω_{HI}, as a function of redshift. Knowledge of the HIMF not only provides information about the H I content of galaxies, but it provides the contextual framework within which other H I studies are conducted, i.e. are the galaxies under investigation chosen from the rare, high-mass end of the distribution, or are they relatively common? Quantifying the parametrization of the HIMF at several redshifts allows us to move beyond the so-called "strawman" surveys, and set realistic guidelines for a combination of survey tiers that results in a coherent dataset which maximizes scientific return while minimizing duplicated effort.

We use the Schechter function parametrization of the HIMF as used by the ALFALFA team in Martin et al. (2010), given by:

$$\phi(M_{HI}) = \frac{dn}{d\log M_{HI}} = \ln 10\, \phi_\star \left(\frac{M_{HI}}{M_\star}\right)^{\alpha+1} e^{-\frac{M_{HI}}{M_\star}} \quad (1)$$

There are three parameters to determine: the faint-end slope α, the characteristic mass $M_\star$, and the normalisation $\phi_\star$. The lack of observational data regarding the detailed distribution of H I content of individual galaxies at $z > 0.2$ provides little constraint on any evolution in the HIMF, so we do not include any evolution in the three parameters. The combination of observing H I in emission at low redshift, and high redshift observations of damped Lyα absorption seen in the spectra of background quasars constrains the evolution of $\Omega_{\rm HI}$ to be at most a factor of a few between $0 < z < 2$, so we do not expect drastic evolution of the individual HIMF parameters over our redshift range of interest, $0 < z < 1.4$. Simulations from Davé et al. (2013) indicate that the high mass end of their HIMF steepens significantly, but only at high redshifts, $z > 2$.

We construct HIMFs from the combinations of surveys introduced in Section 3.1 and see how the different surveys provide complementary constraints. As an illustration, the advantage gained from combining surveys of different depth and area is displayed in Fig. 7, which shows the HIMF resulting from the MIGHTEE and LADUMA surveys individually, and the result from combining the data. The uncertainties on the individual HIMFs from LADUMA and MIGHTEE are $1/\sqrt{N}$, where N is the number of objects in the given mass bin of width ΔLog(M) = 0.1. These are represented by the shaded areas in the main panel, and the final combined HIMF is shown in black with errorbars. The large volume covered by MIGHTEE is entirely responsible for constraining the high-mass end of the HIMF, as LADUMA does not contain any of these rare galaxies. At the low-mass end, the deep flux limit of LADUMA is required, and a small mass range around the break in the relation is covered by both surveys. When combined, the three parameters describing the HIMF are better constrained than considering each survey individually.

Fig. 8 compares the HIMF that can be constructed from the Optimised surveys and either of the Ideal options, at $0.2 < z < 0.3$. For the top panel, the existing Band 1 does not cover redshifts below $z < 0.35$, so the UD component is excluded. The break and the high-mass end of the HIMF are well constrained by the MW and W survey components, as seen by the small uncertainties. Alternatively, the Ideal cases in the bottom panel do incorporate the UD component, which has large uncertainties at high H I masses, but extends the HIMF to lower masses, helping constrain the low-mass slope.

At higher redshift, $0.35 < z < 0.45$, Fig. 9 shows that the Optimised and either of the Ideal surveys both incorporate the UD component, but lose significant contribution from the W survey, which only detects galaxies in the final few H I mass bins. The short vertical line in the top panel indicates the limiting H I mass reached if the sensitivity of the current Band 1 receiver is reduced by a factor of two. The bottom panel shows that the larger area of the Ideal MW tier reduces the uncertainties at the high-mass end of the HIMF. If we allow the normalization of the HIMF to evolve with redshift such that by $z = 1$ the integral is twice that at $z = 0$, we get the dashed curve shown in the bottom panel of Fig. 9. The uncertainties in the HIMF determination for both cases are sufficiently small to distinguish between the evolving and non-evolving cases.

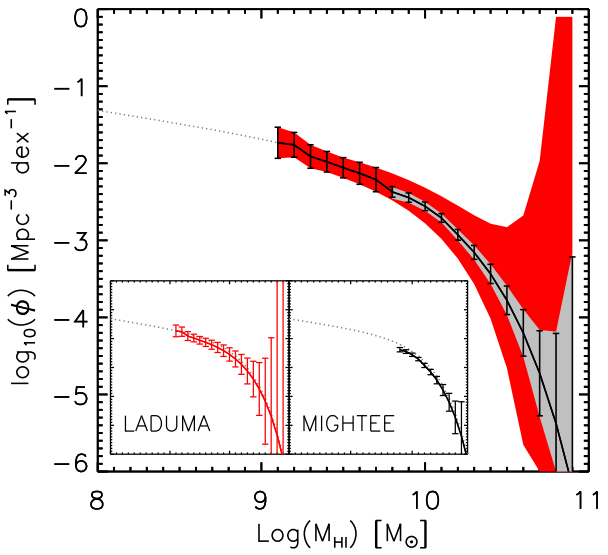

Figure 7. The HIMF resulting from combining H I data from MIGHTEE and LADUMA at $0.1 < z < 0.2$. The two insets show the HIMF from MIGHTEE and LADUMA individually, and the main panel shows is the combination of the two. The x-axis in the main panel and the insets span the same range. The grey region is the HIMF from MIGHTEE including uncertainties, the red region is from LADUMA with the associated uncertainties, and the black line with errorbars is the combination of the two. The dotted grey line here and in the following figures is the input $z = 0$ HIMF from ALFALFA, for reference.

4 COMPLEMENTARITY OF H I AND CONTINUUM SURVEYS

The benefits of observing commensally to minimize observational effort while maximizing science return are clear. Provided sufficient advance effort with respect to survey design and science requirements is invested, it is possible to construct a coherent dataset from disparate surveys. With a major scientific effort such as the SKA, the accessibility of previously unexplored parameter space is expected to transform our understanding of a number of key areas of astrophysics, so we must ensure we undertake surveys which will provide the data needed to significantly advance our current knowledge.

Here we explore the *complementarity* of the data products resulting from the commensal H I and radio continuum observations, biases in the resulting dataset, limitations resulting from restricted sensitivity at different wavelengths, and how information can be combined to circumvent these limitations.

4.1 Low redshift H I and Optical Data

With future observations, we will have simultaneous measures of both the H I reservoirs of galaxies, along with star formation rate indicators from the radio continuum, over a cosmological redshift range. Our current information, particularly H I, is restricted to $z \sim 0$. While limited, the existing data can be used to provide the context within which we can expect the new observations to fit.

To understand how H I, optical and radio continuum

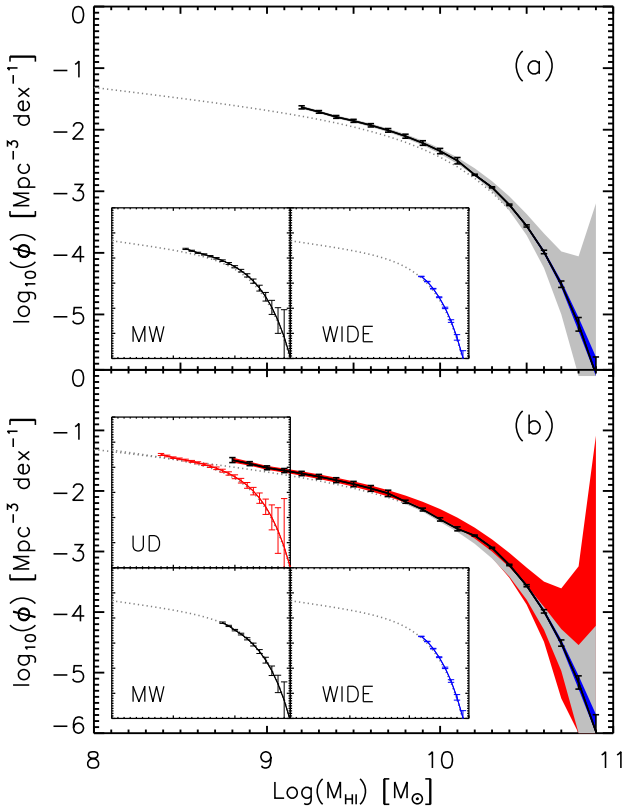

Figure 8. The HIMF resulting from combining H I data from the MW (grey) and W (blue) components of the Optimised survey (top panel), and the UD (red), MW (grey) and W (blue) components of the Ideal surveys (bottom panel), both at $0.2 < z < 0.3$. The UD component is not included in the top panel as Band 1 does not extend to these low redshifts. The addition of the UD component in the bottom panel shows the HIMF can be probed to lower masses. The x-axis in the main panel and the insets span the same range.

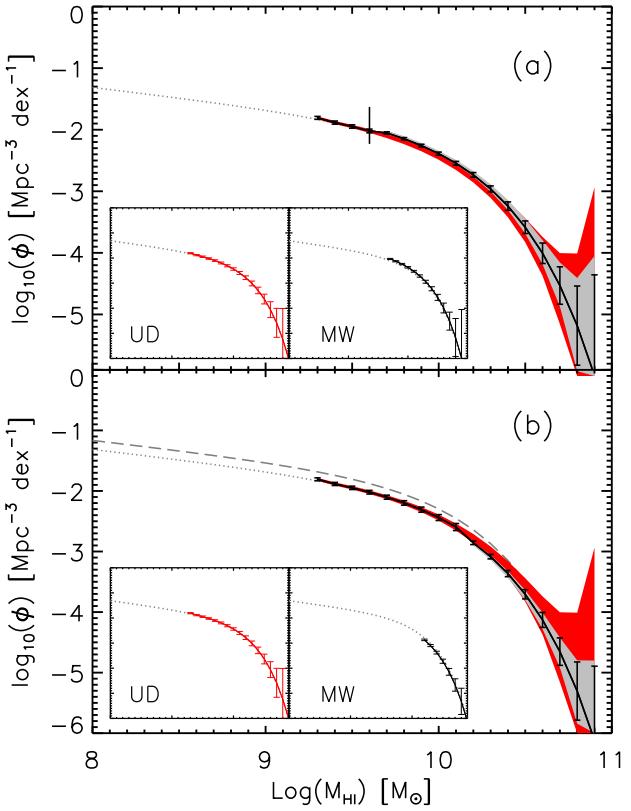

Figure 9. The HIMF resulting from combining H I data from the UD (red) and MW (grey) components of the Optimised (top panel) and Ideal surveys (bottom panel) at $0.35 < z < 0.45$. The larger area of the MW component in Ideal compared to the Optimised case improves the constraints at the high-mass end. The short vertical line in the top panel marks the limiting H I mass if the sensitivity of the current Band 1 is reduced by a factor of two, and the dashed line in the bottom panel indicates the HIMF if allowed to evolve with redshift. The dotted line is the $z = 0$ HIMF as in previous figures. The x-axis in the main panel and the insets span the same range.

surveys will fit together, we take advantage of the spatial overlap of two individual, large-area surveys. Optical photometry and spectroscopy are provided by the Sloan Digital Sky Survey (SDSS, York et al. 2000). The H I data are from the Arecibo Legacy Fast ALFA survey (ALFALFA, Giovanelli et al. 2005) $\alpha.40$ source catalogue from Haynes et al. (2011), which covers $\sim$2800 deg^2 within the SDSS imaging footprint, and contains 15 041 secure extragalactic sources. ALFALFA is flux-limited to $\sim$0.47 Jy km s^{-1}, while the spectral range allows observations of galaxies to $z = 0.06$. From this catalogue we extract the H I masses, M_{HI}, from the H I profiles, along with the galaxy redshifts provided within the ALFALFA data release.

The ALFALFA team has crossmatched the $\alpha.40$ catalogue to the SDSS Data Release 7 (DR7, Abazajian et al. 2009) by hand to identify the most likely optical counterparts for the H I detections. 11 740 of the ALFALFA galaxies have clear optical counterparts in the DR7 imaging, providing optical photometry, galaxy sizes, and for the majority of the objects, spectroscopic redshifts. We refer to this set of galaxies as the ALFALFA–SDSS sample.

At the intersection of ALFALFA and SDSS, we have, for a large number of galaxies, information regarding the neutral gas reservoir, the existing stellar properties, and a measure of the star formation rate from optical photometry. Even though ALFALFA is restricted to $z < 0.06$, the galaxies contained within the survey span a wide range of H I masses, stellar masses, and star formation rates, and provide a useful low redshift frame of reference for extrapolating to the higher redshifts and greater depths which will be probed by upcoming surveys.

4.2 H I and radio continuum selection of galaxies

As described in detail in Huang et al. (2012), H I selection results in a highly biased galaxy sample, preferentially including blue, star forming objects. Constructing a galaxy sample flux-limited in the radio continuum also results in a biased census, composed of two populations of objects. The high luminosities are dominated by galaxies hosting active galactic nuclei (AGN), whereas at lower luminosities, the star-forming galaxies become more prevalent (for example, Wilman et al. 2008, Padovani et al. 2009, Massardi et al. 2010, McAlpine, Jarvis, & Bonfield 2013). Continuum sur-

veys with flux limits sensitive enough to probe below the AGN regime will have significant numbers of star-forming galaxies, which are the same galaxies selected by deep H I surveys. So although both H I and continuum selection result in biased galaxy samples, they are biased toward the same galaxies.

The galaxy mass function derived from the Galaxy And Mass Assembly (GAMA, Driver et al. 2011) shows that at the highest stellar masses, the galaxy counts are dominated by red galaxies (Baldry et al. 2012), which tend to be H I-poor and have little star formation activity. However, at stellar masses $M_* < 10^{10.3}\,M_\odot$, the galaxy counts are dominated by blue galaxies, which is also where the bulk of star formation activity occurs, and is exactly the population of objects both H I and continuum selection are biased toward.

4.3 Optical Imaging and Spectroscopy

A multi-wavelength aspect, combining several individual surveys at different wavelengths, is becoming increasingly common with current and future surveys, including upcoming radio-based observations. These ancillary data, primarily optical imaging and spectroscopy, provide additional information for the galaxy population under examination. However, the optical observations impose their own flux limits on a given survey in addition to the H I and continuum sensitivities imposed by the radio wavelength observing parameters. Imaging large areas of sky to significant depths in order to obtain galaxy colours and morphological information is well within the capabilities of current optical instrumentation, as proven by, for example, the Canada-France-Hawaii Telescope Legacy Survey (CFHTLS[7]), the Cosmic Evolution Survey (COSMOS, Scoville et al. 2007), UltraVISTA (McCracken et al. 2012), the VISTA Deep Extragalactic Observations survey (VIDEO, Jarvis et al. 2013), and Dark Energy Survey (DES[8]) and do not impose significant limitations on the galaxy sample to be observed. Upcoming surveys such as the Large Synoptic Survey Telescope (LSST, Ivezic et al. 2008), Euclid (Laureijs et al. 2012), and WFIRST[9] actively incorporate surveys at other wavelengths in their planning strategy.

Large area, flux-limited spectroscopic surveys, however, require extensive telescope time and effort. While photometric redshifts (photo-z), with accuracies of $\Delta z \sim 0.05$ are sufficient for a number of scientific applications (the evolution of luminosity functions, for example), the accuracy of spectroscopic redshifts ($\Delta z \sim 0.0003$) are required for investigations of detailed galaxy environment and spectral stacking (Maddox et al. 2013). The acquisition of sufficient spectroscopic redshifts to supplement upcoming H I and continuum surveys is the topic of much discussion and effort (see a good overview in Meyer et al. 2015), and here we investigate the effect of imposing an optical flux limit on a galaxy sample initially flux-limited in H I as a function of redshift, and what other information we can use to alleviate the effects.

[7] http://www.cfht.hawaii.edu/Science/CFHTLS/
[8] http://www.darkenergysurvey.org
[9] http://wfirst.gsfc.nasa.gov

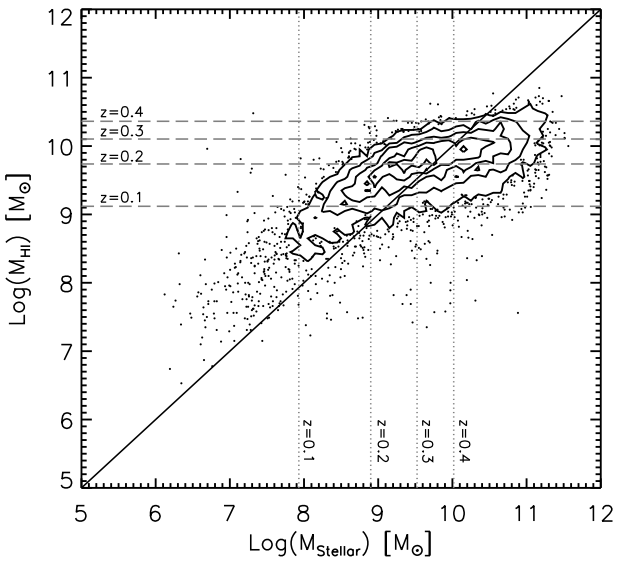

Figure 10. M_{HI} as a function of M_* for the ALFALFA–SDSS galaxies, in units of $M_\odot$. The diagonal black solid line marks the 1-to-1 relation. The vertical grey dotted lines indicate the stellar mass limits resulting from an optical flux limit of $r = 22$ at various redshifts as described in Section 4.3, while the horizonal grey dashed lines indicate the H I mass sensitivity of the CHILES survey at $z = 0.1 - 0.4$, outlined in Section 4.5.

4.3.1 Scaling Relations and Flux Limits

Scaling relations illustrate general trends between physical properties for an ensemble of galaxies. One such relation at $z \sim 0$ is shown in Fig. 10, indicating how H I mass, from the ALFALFA catalogue, and stellar mass, from the MPA–JHU catalogue (Brinchmann et al. 2004, Tremonti et al. 2004), are related for the H I-selected ALFALFA–SDSS galaxies. At low stellar masses, below $M_* < 10^9\,M_\odot$, the galaxies are H I-rich, lying above the diagonal line marking the 1-to-1 relation. At high stellar masses, the galaxies become increasingly H I-poor. Extensive discussion regarding the features of this relation can be found in Maddox et al. (2015). There are many galaxies not detected by ALFALFA which would lie in the bottom right corner of Fig. 10, at high stellar mass and low H I mass. These are the absent red sequence galaxies not included in an H I-selected sample. While a small number of early-type galaxies are found to have significant masses of H I (Serra et al. 2012), the contribution from these galaxies to the H I mass census is negligible.

Known scaling relations can also be useful for converting observable quantities, such as brightness, into quantities that are difficult to measure either directly or indirectly. For example, a galaxy's stellar content can be estimated using only it's brightness and colour by employing the known correlation between the optical luminosity and colours of a galaxy and its stellar mass (Bell et al. 2003). We use this relation to convert optical flux limits to approximate limiting stellar masses, as a function of redshift, to illustrate the effect these flux limits have on an H I-selected galaxy sample.

Due to the biased nature of the ALFALFA–SDSS galaxies, we derive a Luminosity–M_* relation specifically for this dataset. As the H I-selected galaxies are nearly all blue cloud galaxies, we remove the colour dependence of the usual

Luminosity–M_* relation by assuming all galaxies have the same representative colour. This approximation is sufficient for the illustration presented here. We find:

$$\mathrm{Log}(M_*) = -0.546(M_r) - 1.051 \quad (2)$$

where M_* is in units of solar masses, and M_r is the absolute r-band magnitude. We then use this relation to convert a given optical flux limit into an approximate redshift-dependent stellar mass limit, incorporating a k-correction appropriate for blue galaxies. The calculation is only an approximation, because it uses the relation derived from the $z = 0$ population and assumes no evolution with redshift.

Shown on Fig. 10 are vertical lines indicating the effective stellar mass limits resulting from imposing a flux limit of $r < 22$, appropriate for an optical spectroscopic campaign, on the $z = 0$ H I-selected galaxy ensemble. The distribution of galaxies in this figure is to provide the low redshift reference for the populated regions of parameter space, which will evolve with redshift in an unknown way, as we currently cannot make such a figure at $z > 0$. The limits at increasing redshift then illustrate which parts of the parameter space are no longer accessible.

At $z = 0.1$, all galaxies with $M_* > 10^8\,M_\odot$ are brighter than $r = 22$, but galaxies are rapidly lost with increasing redshift, leaving only objects with $M_* > 10^{10}\,M_\odot$ bright enough for spectroscopy at $z = 0.4$. Note that these limits ignore the complicating factor of galaxy surface brightness, which works against observations of disk galaxies, particularly when viewed face-on. Relaxing the optical flux limit to $r = 24$, more appropriate for optical photometry alone, shifts the effective stellar mass limits lower by an order of magnitude. This fainter flux limit is relevant for obtaining photometric redshifts with current facilities over moderately wide areas.

Also shown on Fig. 10 are horizontal lines denoting the 5-σ H I mass sensitivity of CHILES as a function of redshift (see Section 4.5 for details). The important detail to note is that for a given H I mass, for example $M_{HI} = 10^9\,M_\odot$, the stellar masses range from $10^8 < M_* < 10^{11}\,M_\odot$. Even at $z = 0.3$, galaxies of $M_* \sim 10^9\,M_\odot$ will be detected in the most H I-rich cases, a factor of more than three lower in stellar mass than is accessible to optical spectroscopy at the same redshift, unless the objects have very strong emission lines. Thus, selection to a given H I flux limit is effective at identifying galaxies with a wide range of stellar masses, whereas selection incorporating an optical flux limit is strongly biased toward the most massive stellar systems, particularly at increasing redshift. In fact, the H I observations themselves are able to provide redshifts for these galaxies below the stellar masses accessible to optical spectroscopy.

4.4 Continuum and Spectral Stacking

In order to explore the average galaxy population below the detection threshold of a given survey, statistical co-adding, or stacking, is often employed. Stacking in the radio continuum has been successfully performed by a number of authors (for example, White et al. 2007, Garn & Alexander 2009, Karim et al. 2011, Zwart, Santos, & Jarvis 2015, or see Zwart et al. 2015 for a good overview). The spatial coordinates of the galaxies are provided by deep optical or near-infrared imaging, and redshifts are required to convert fluxes into luminosities.

With the commensal H I and continuum observations, the galaxy population selected in H I, rather than at optical wavelengths, can be used as the basis for a star formation census over the redshift range probed by the spectral observations. Not only does the H I selection provide a galaxy sample less biased by stellar mass, but the H I detections themselves provide the redshifts of the galaxies, without the need for additional expensive spectroscopy, which quickly becomes unfeasible for large numbers of galaxies with $M_* \sim 10^9\,M_\odot$ at $z > 0.2$.

4.5 Case study: CHILES and CHILES Con Pol

As described in Section 4.2, observations in H I and radio continuum tend to select the same galaxy population, so within a single observation, we gain information about both the neutral gas content and star formation activity in the same set of galaxies. We investigate a pair of complementary spectral line and radio continuum surveys currently underway with the VLA.

The COSMOS H I Large Extragalactic Survey (CHILES[10]) project is a deep, 1000 hour observation of a single pointing. The instantaneous frequency coverage of 1450–970 MHz allows H I detections over the unprecedented redshift range $0 < z < 0.45$, which will only be surpassed by SKA-era facilities. Two semesters of observations are already completed, and the feasibility is demonstrated by the pilot project, spanning $0 < z < 0.193$ (Fernández et al. 2013). The same 1000 hours of observations are being shared with the CHILES Continuum Polarization (CHILES Con Pol[11], Hales & Chiles Con Pol Collaboration 2014) team, who are exploiting the flexibility and power of the upgraded VLA correlator to simultaneously observe in four 128 MHz continuum bands to create a deep continuum map of the same area of sky.

The total observing time for CHILES was chosen in order to detect a galaxy with $M_{HI} \sim 3 \times 10^{10}\,M_\odot$ at the highest accessible redshift. This corresponds to a 5-σ flux limit of 0.0295 Jy km s^{-1}, which translates directly to a redshift-dependent H I mass limit via:

$$M_{\mathrm{HI}} = 2.356 \times 10^5\, D_L^2\, (1+z)^{-1} \int S_\nu\, dv \quad (3)$$

where M_{HI} is in solar masses, the luminosity distance to the galaxy, D_L, is in Mpc, and the integral is the total flux in Jy km s^{-1}. The $(1+z)$ factor accounts for the difference between the observed and rest-frame profile width. Assuming an H I profile width of 150 km s^{-1}, the minimum detectable H I mass at $z =$ 0.1, 0.2, 0.3 and 0.4 are marked as horizontal dashed lines on Fig. 10. At $z = 0.1$, galaxies with $M_{HI} \sim 10^9\,M_\odot$ are easily detectable, thus including the bulk of the H I mass. The stellar masses for these galaxies spans $10^8 < M_* < 10^{11}\,M_\odot$. Even at $z = 0.2$, the H I mass limit is still below the break mass of the $z = 0$ H I mass function, at $10^{9.96}\,M_\odot$ (Martin et al. 2010).

In reality, these mass limits have some variation for a

[10] http://chiles.astro.columbia.edu/
[11] http://www.chilesconpol.com

given flux limit, as the resulting detection limit is dependent on the HI profile width, as determined by not only the mass of the galaxy, but it's inclination to the line of sight. For a given flux limit, galaxies seen face-on can be detected to lower mass limits than galaxies viewed edge-on, by about 0.3 dex. Thus, a flux limit doesn't result in a hard lower mass limit, but rather a lower mass limit with a decreasing number of galaxies to lower masses seen increasingly face-on. The limiting H I masses marked on Fig. 10 should then only be used for guidance.

In a similar manner to H I, the expected flux limit of 0.6μJy per beam in continuum for CHILES Con Pol can be converted to an equivalent detectable star formation rate as a function of redshift. To convert the 1.4 GHz continuum flux, f, into luminosity, we use:

$$L = \frac{f D_L^2 (1+z)^{\alpha-1}}{1 \times 10^{26}} \quad (4)$$

where the luminosity, L, is in W Hz^{-1} sr^{-1} and assuming a power-law spectral index $S_\nu \propto \nu^{-\alpha}$ and $\alpha = 0.7$. Then, using the relation to convert 1.4 GHz luminosity to a star formation rate, we use the relation from Murphy et al. (2011):

$$\mathrm{SFR}(\mathrm{M}_\odot\ yr^{-1}) = 4\pi\ 6.35 \times 10^{-22} L \quad (5)$$

Even at $z = 0.4$, CHILES Con Pol will be sensitive enough to detect star formation rates of ~ 1 M$_\odot$ year^{-1}. Thus, for the first time, we will have information about moderate levels of star formation, along with the H I reservoirs, in galaxies over a range of redshifts. Due to the computing capacities now available, this information can be collected with one set of observations.

With the relatively small field of view of the VLA, $\sim$0.5 deg in diameter, and restricted redshift range of $0 < z < 0.5$ for H I, the number of galaxies contained within the observed volume is manageably small, on the order of 300 galaxies. The CHILES pointing is within the COSMOS footprint, thus deep multi-wavelength imaging (Scoville et al. 2007, McCracken et al. 2012), along with extensive spectroscopy, already exist (Lilly et al. 2007, Lilly et al. 2009, Garilli et al. 2008, Coil et al. 2011, Cool et al. 2013, Ahn et al. 2014). These catalogues have been conveniently amalgamated, and for the zCOSMOS spectra, reprocessed, by Davies et al. (2015). This indicates the amount of ancillary data required to support upcoming radio surveys. With the larger fields of view and wider frequency coverage of SKA-era facilities, the ancillary data effort becomes even more substantial.

5 SUMMARY

Despite H I ultimately providing the raw material required for star formation, little is known about how galaxies acquire and consume this fuel over cosmological timescales. Conversely, the star formation density in the Universe has been traced with a number of techniques to the highest observable redshifts. With current and upcoming radio facilities, enabled by advances in engineering and computing, we will, for the first time, be able to trace both the H I reservoir and the star formation activity in the same galaxies over a cosmologically significant timescale, when the SFR is dropping rapidly but the neutral gas content remains relatively stable.

Careful planning of commensal observations enables multiple science cases to benefit from the same data, and maximises the scientific return with no impact on telescope time. The MeerKAT programmes LADUMA and MIGHTEE are an excellent example of survey tiers well matched in terms of relative depth and area coverage, creating a comprehensive H I dataset. Conversely, the three H I survey tiers suggested by the SKA H I science working group to be undertaken with the SKA1-MID instrument require significant rearrangement in terms of area and depth to create a coherent dataset. The definition of the frequency bands is a critical aspect when designing the tiered survey, especially for H I science. We find that alternative frequency band definitions, either the suggested alteration of Bands 1 and 2, or a new single-octave band covering 1200–600MHz, require less extreme survey tiers, and less observing time, in order to optimally cover the redshift–M_{HI} parameter space.

In addition to H I and continuum observations being highly commensal, the data products are also complementary. H I selection results in a galaxy sample biased toward blue, star-forming galaxies, which are the same galaxies that dominate radio continuum selection at faint flux limits. H I selection also results in a sample less biased in terms of stellar mass than the effective optical flux limit that results from the additional requirement of obtaining spectroscopic redshifts. In fact, data from the radio spectral line observations are able to provide redshifts for gas-rich galaxies without needing additional optical spectroscopy.

Commensal observing will become more common as new facilities with expanded capabilities come online, and large programmes compete for ever increasing time allocations. Maximising the science return for many separate projects while minimising observational effort will be essential to achieve the ambitious goals set out by each team, whose individual survey plans would not be realised otherwise. The current investigation shows that with adjustments of survey parameters, including area and depth, a coherent strategy satisfying several communities is possible, provided advance effort is committed to the planning stages.

ACKNOWLEDGEMENTS

The Arecibo Observatory is operated by SRI International under a cooperative agreement with the National Science Foundation (AST-1100968), and in alliance with Ana G. Méndez-Universidad Metropolitana, and the Universities Space Research Association. We acknowledge the work of the entire ALFALFA collaboration team in observing, flagging, and extracting the catalogue of galaxies used in this work.

Funding for the SDSS and SDSS-II was provided by the Alfred P. Sloan Foundation, the Participating Institutions, the National Science Foundation, the U.S. Department of Energy, the National Aeronautics and Space Administration, the Japanese Monbukagakusho, the Max Planck Society, and the Higher Education Funding Council for England. The SDSS was managed by the Astrophysical Research Con-

sortium for the Participating Institutions. The SDSS Web Site is http://www.sdss.org/.

The SDSS is managed by the Astrophysical Research Consortium for the Participating Institutions. The Participating Institutions are the American Museum of Natural History, Astrophysical Institute Potsdam, University of Basel, University of Cambridge, Case Western Reserve University, University of Chicago, Drexel University, Fermilab, the Institute for Advanced Study, the Japan Participation Group, Johns Hopkins University, the Joint Institute for Nuclear Astrophysics, the Kavli Institute for Particle Astrophysics and Cosmology, the Korean Scientist Group, the Chinese Academy of Sciences (LAMOST), Los Alamos National Laboratory, the Max-Planck-Institute for Astronomy (MPIA), the Max-Planck-Institute for Astrophysics (MPA), New Mexico State University, Ohio State University, University of Pittsburgh, University of Portsmouth, Princeton University, the United States Naval Observatory, and the University of Washington. This research has made use of NASA's Astrophysics Data System.

This work has benefitted from useful discussions, particularly with Ian Heywood and Chris Hales. MJJ acknowledges support from SKA South Africa and STFC. We thank the anonymous referee for helpful comments which improved this paper.

REFERENCES

Abazajian K. N., et al., 2009, ApJS, 182, 543
Ahn C. P., et al., 2014, ApJS, 211, 17
Baldry I. K., et al., 2012, MNRAS, 421, 621
Barnes D. G., et al., 2001, MNRAS, 322, 486
Bell E. F., McIntosh D. H., Katz N., Weinberg M. D., 2003, ApJS, 149, 289
Blyth S., et al., 2015, Proceedings of Advancing Astrophysics with the Square Kilometre Array (AASKA14). 9–13 June, 2014. Giardini Naxos, Italy. Online at http://pos.sissa.it/cgi-bin/reader/conf.cgi?confid=215,%20id.128
Braun R., Bourke T., Green J. A., Keane E., Wagg J., 2015, Proceedings of Advancing Astrophysics with the Square Kilometre Array (AASKA14). 9–13 June, 2014. Giardini Naxos, Italy. Online at http://pos.sissa.it/cgi-bin/reader/conf.cgi?confid=215,%20id.174
Brinchmann J., Charlot S., White S. D. M., Tremonti C., Kauffmann G., Heckman T., Brinkmann J., 2004, MNRAS, 351, 1151
Catinella B., Cortese L., 2015, MNRAS, 446, 3526
Coil A. L., et al., 2011, ApJ, 741, 8
Condon J. J., et al., 2012, ApJ, 758, 23
Cool R. J., et al., 2013, ApJ, 767, 118
Davé R., Katz N., Oppenheimer B. D., Kollmeier J. A., Weinberg D. H., 2013, MNRAS, 434, 2645
Davies L. J. M., et al., 2015, MNRAS, 447, 1014
Driver S. P., et al., 2011, MNRAS, 413, 971
Fernández X., et al., 2013, ApJ, 770, LL29
Garilli B., et al., 2008, A&A, 486, 683
Garn T., Alexander P., 2009, MNRAS, 394, 105
Giovanelli R., et al., 2005, AJ, 130, 2598
Hales C. A., Chiles Con Pol Collaboration, 2014, Exascale Radio Astronomy, 50301
Haynes M. P., et al., 2011, AJ, 142, 170
Heywood I., Jarvis M. J., Condon J. J., 2013, MNRAS, 432, 2625
Holwerda B. W., Blyth S.-L., Baker A. J., Baker, 2012, IAUS, 284, 496
Hopkins A. M., Beacom J. F., 2006, ApJ, 651, 142
Huang S., Haynes M. P., Giovanelli R., Brinchmann J., 2012b, ApJ, 756, 113
Ivezic Z., et al., 2008, arXiv, arXiv:0805.2366
Jaffé Y. L., Poggianti B. M., Verheijen M. A. W., Deshev B. Z., van Gorkom J. H., 2013, MNRAS, 431, 2111
Jarvis M. J., 2012, African Skies, 16, 44
Jarvis M. J., et al., 2013, MNRAS, 428, 1281
Jarvis M., Bacon D., Blake C., Brown M., Lindsay S., Raccanelli A., Santos M., Schwarz D. J., 2015, Proceedings of Advancing Astrophysics with the Square Kilometre Array (AASKA14). 9–13 June, 2014. Giardini Naxos, Italy. Online at http://pos.sissa.it/cgi-bin/reader/conf.cgi?confid=215,%20id.18
Johnston S., et al., 2008, ExA, 22, 151
Jonas J. L., 2009, IEEEP, 97, 1522
Karim A., et al., 2011, ApJ, 730, 61
Komatsu E., et al., 2011, ApJS, 192, 18
Lah P., et al., 2007, MNRAS, 376, 1357
Laureijs R., et al., 2012, SPIE, 8442, 84420T
Lilly S. J., et al., 2007, ApJS, 172, 70
Lilly S. J., et al., 2009, ApJS, 184, 218
Maddox N., Hess K. M., Blyth S.-L., Jarvis M. J., 2013, MNRAS, 433, 2613
Maddox N., Hess K. M., Obreschkow D., Jarvis M. J., Blyth S.-L., 2015, MNRAS, 447, 1610
Martin A. M., Papastergis E., Giovanelli R., Haynes M. P., Springob C. M., Stierwalt S., 2010, ApJ, 723, 1359
Massardi M., Bonaldi A., Negrello M., Ricciardi S., Raccanelli A., de Zotti G., 2010, MNRAS, 404, 532
McAlpine K., Jarvis M. J., Bonfield D. G., 2013, MNRAS, 436, 1084
McCracken H. J., et al., 2012, A&A, 544, A156
Meyer M., Robotham A., Obreschkow D., Driver S., Staveley-Smith L., Zwaan M., 2015, Proceedings of Advancing Astrophysics with the Square Kilometre Array (AASKA14). 9–13 June, 2014. Giardini Naxos, Italy. Online at http://pos.sissa.it/cgi-bin/reader/conf.cgi?confid=215,%20id.131
Meyer M. J., et al., 2004, MNRAS, 350, 1195
Murphy E. J., et al., 2011, ApJ, 737, 67
Noterdaeme P., et al., 2012, A&A, 547, LL1
Obreschkow D., Klöckner H.-R., Heywood I., Levrier F., Rawlings S., 2009, ApJ, 703, 1890
Oosterloo T., Verheijen M. A. W., van Cappellen W., Bakker L., Heald G., Ivashina M., 2009, arXiv, arXiv:0912.0093
Padovani P., Mainieri V., Tozzi P., Kellermann K. I., Fomalont E. B., Miller N., Rosati P., Shaver P., 2009, ApJ, 694, 235
Popping A., Meyer M., Staveley-Smith L., Obreschkow D., Jozsa G., Pisano D. J., 2015, Proceedings of Advancing Astrophysics with the Square Kilometre Array (AASKA14). 9–13 June, 2014. Giardini Naxos, Italy. Online at http://pos.sissa.it/cgi-bin/reader/conf.cgi?confid=215,%20id.132
Prandoni I., Seymour N., 2015, Proceedings of Advancing Astrophysics with the Square Kilometre Array (AASKA14). 9–13 June, 2014. Giardini Naxos, Italy. Online at http://pos.sissa.it/cgi-bin/reader/conf.cgi?confid=215,%20id.67
Rhee J., Zwaan M. A., Briggs F. H., Chengalur J. N., Lah P., Oosterloo T., van der Hulst T., 2013, MNRAS, 435, 2693
Scoville N., et al., 2007, ApJS, 172, 1
Serra P., et al., 2012, MNRAS, 422, 1835
Spergel D. N., et al., 2003, ApJS, 148, 175
Staveley-Smith L., Oosterloo T., 2015, Proceedings of Advancing Astrophysics with the Square Kilometre Array (AASKA14). 9–13 June, 2014. Giardini Naxos, Italy. Online at http://pos.sissa.it/cgi-bin/reader/conf.cgi?confid=215,%20id.167
Tremonti C. A., et al., 2004, ApJ, 613, 898
White R. L., Helfand D. J., Becker R. H., Glikman E., de Vries W., 2007, ApJ, 654, 99
Wilman R. J., et al., 2008, MNRAS, 388, 1335

York D. G., et al., 2000, AJ, 120, 1579
Zwart J., et al., 2015, Proceedings of Advancing Astrophysics with the Square Kilometre Array (AASKA14). 9–13 June, 2014. Giardini Naxos, Italy. Online at http://pos.sissa.it/cgi-bin/reader/conf.cgi?confid=215,%20id.172
Zwart J. T. L., Santos M., Jarvis M. J., 2015, MNRAS, 453, 1740

This paper has been typeset from a TEX/LATEX file prepared by the author.